Antiferromagnetic rare-earth ordering in the intermetallic compounds R_2Pd_2In (R = Pr, Nd)

2000 J. Phys.: Condens. Matter 12 7089

(http://iopscience.iop.org/0953-8984/12/31/310)

J. Phys.: Condens. Matter **12** (2000) 7089–7098. Printed in the UK PII: S0953-8984(00)13119-4

Antiferromagnetic rare-earth ordering in the intermetallic compounds R_2Pd_2In (R = Pr, Nd)

P Fischer†‖, T Herrmannsdörfer†, T Bonelli†, F Fauth†¶, L Keller†, E Bauer‡ and M Giovannini§

† Laboratory for Neutron Scattering, ETH Zürich and Paul Scherrer Institute, CH-5232 Villigen PSI, Switzerland
‡ Institut für Experimentalphysik, TU Wien, A-1040 Vienna, Austria
§ Dipartimento di Chimica e Chimica Industriale, Università di Genova, I-16146 Genova, Italy

E-mail: Peter.Fischer@psi.ch

Received 7 April 2000

Abstract. The intermetallic compounds R_2Pd_2In of the light rare earths R = Pr, Nd were investigated by means of powder neutron diffraction in the temperature range from 1.6 K to 15 K. The chemical structure is of Mo_2FeB_2 type according to the space group $P4/mbm$. Antiferromagnetic rare-earth ordering of modulated type corresponding to $\boldsymbol{k} = [0, 0, 1/2]$ and $[1/4, 1/4, 0]$ was established below the Néel temperatures $T_N = 5$ K and 8 K for R = Pr and Nd, respectively, in contrast to $\boldsymbol{k} \approx [0.22, 0, 0]$ and $\boldsymbol{k} = [0, 0, 0]$ of the antiferromagnetic and ferromagnetic, nonstoichiometric Ce_2Pd_2In systems.

1. Introduction

The compounds R_2Pd_2In (R = rare earth) form an isostructural series with tetragonal Mo_2FeB_2 type structure (space group $P4/mbm$). From systematic bulk magnetic measurements one observes a large variation of the magnetic properties, presumably due to the lanthanide contraction in connection with RKKY exchange interactions and crystal field effects [1]. With the exception of Ce, Sm and Yb, the effective magnetic moments are close to the free ion values of trivalent rare earths. Tb_2Pd_2In displays the largest Néel temperature $T_N = 32$ K, whereas Pr_2Pd_2In and Nd_2Pd_2In order antiferromagnetically at $T_N = 5$ K and 8 K, respectively. Different 'de Gennes scaling' was found for the light and heavy rare earths, and the Tb compound appears to be anomalous in this respect. The electrical resistivity of Ce_2Pd_2In shows features of Kondo type interaction. This system is particularly interesting, as it exhibits an extended solid solubility range, and the magnetic properties are critically influenced by the chemical composition, changing from ferro- to antiferromagnetism. By means of neutron diffraction the antiferromagnetism was recently shown to be of modulated type with propagation vector $\boldsymbol{k} \approx [0.22, 0, 0]$ [2]. Yb_2Pd_2In exhibits intermediate valent behaviour without magnetic order down to 0.3 K.

In the context of a systematic neutron diffraction determination of magnetic ordering in strongly correlated electron systems, we present here the results for the isostructural R_2Pd_2In

‖ Corresponding author: Dr P Fischer, Laboratory for Neutron Scattering, ETH Zurich and Paul Scherrer Institute, WHGA/133, CH-5232 Villigen PSI, Switzerland.
¶ Present address: SLS, Paul Scherrer Institute, CH-5232 Villigen PSI, Switzerland.

0953-8984/00/317089+10$30.00

compounds of the light rare earths R = Pr and Nd. It will be shown that this series displays a remarkable variation of magnetic ordering.

2. Experiment

Rather large polycrystalline samples were prepared as already described in [1]. No secondary phases were found from x-ray diffraction measurements.

Elastic neutron scattering experiments were performed on the high-resolution powder diffractometer D1A (neutron wavelength $\lambda = 0.1911$ nm) and on the high-intensity powder diffractometers D1B ($\lambda = 0.252$ nm) at the high-flux reactor of Institut Laue–Langevin (ILL), Grenoble and DMC, situated at a supermirror coated guide for cold neutrons at the Swiss spallation neutron source SINQ of the Paul Scherrer Institute (PSI), Villigen ($\lambda = 0.422$ nm, Be filter). The powder samples of nominal compositions Pr_2Pd_2In and Nd_2Pd_2In were enclosed under He gas atmosphere in cylindrical V tubes of 8 mm diameter and of approximately 5 cm height. For $\lambda = 0.422$ nm a similar Al sample container was used. The samples were cooled by means of ILL-type He flow cryostats. According to the measured neutron transmission, absorption corrections were included in the calculations (product of linear absorption coefficient μ and of sample radius r: $\mu r = 0.415$ and 0.281 for the Pr and Nd samples, respectively for neutron wavelength $\lambda = 0.1911$ nm). Refinements of the neutron diffraction data were made by means of the program FullProf [3], using the internal tables of neutron scattering lengths and magnetic form factors.

3. Low-temperature chemical structures

Using the D1A, powder samples of nominal composition R_2Pd_2In (R = Pr, Nd) were investigated at 10 K and 15 K, respectively, in the paramagnetic state. Corresponding neutron diffraction patterns are shown in figures 1 and 2, respectively. To a good approximation (in the case of Nd_2Pd_2In the largest unidentified impurity peak is observed at a scattering angle

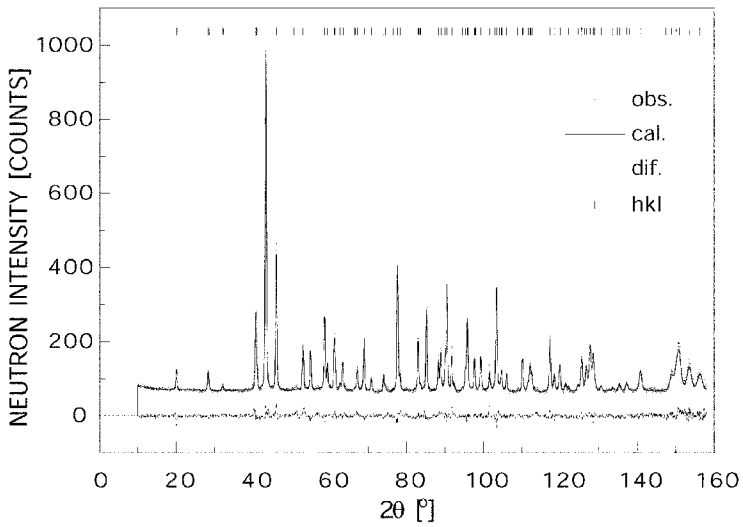

Figure 1. Observed, calculated and difference neutron diffraction patterns of paramagnetic Pr_2Pd_2In at $T = 10$ K. The vertical bars at the top indicate Bragg peak positions.

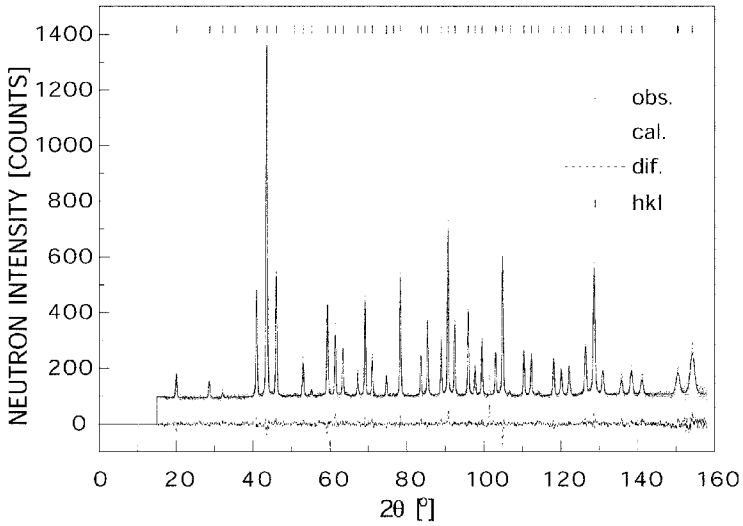

Figure 2. Observed, calculated and difference neutron diffraction patterns of paramagnetic Nd_2Pd_2In at $T = 15$ K.

Table 1. Structural parameters of Pr_2Pd_2In, refined according to space group $P4/mbm$ from neutron diffraction data taken at $T = 10$ K. Lattice parameters $a = 0.7725(1)$ nm, $c = 0.3906(1)$ nm. B = isotropic temperature factor, occupation numbers 100% assumed, goodness of fit $\chi^2 = 2.44$, agreement value $R_{wp} = 5.16\%$ concerning weighted profile intensities, $R_I = 6.62\%$ concerning integrated neutron intensities, expected value from counting statistics $R_{exp} = 3.30\%$, 87 inequivalent reflections (hkl) contributing. Estimated standard deviations are given within parentheses.

Atom	Site	x	y	z	B [10^{-2} nm^2]
Pr	4h	0.1761(1)	0.6761(1)	0.5	0.50(4)
Pd	4g	0.3718(1)	0.8718(1)	0	0.30(3)
In	2a	0	0	0	0.62(5)

Table 2. Interatomic distances Pr–X [nm] in Pr_2Pd_2In, calculated from table 1.

Pr–2Pd	0.2896	Pr–Pr	0.3848
Pr–4Pd	0.3078	Pr–2Pr	0.3906
Pr–4In	0.3453	Pr–4Pr	0.4028

$2\theta \approx 102^\circ$, see figure 2) the specimens appear to be single phase materials of Mo_2FeB_2 type structure with space group symmetry $P4/mbm$ similar to the case at room temperature [1]. The structural results of Rietveld profile refinements, as well as the corresponding shortest interatomic distances, are summarized in tables 1–4. Figure 3 illustrates the chemical structure of Nd_2Pd_2In. Note the distorted triangles of rare earth ions, indicating substantial frustration concerning magnetic interactions. There are one shortest (0.3839 nm) and two longer (0.4026 nm) Nd–Nd distances per triangle. The latter distance holds also for the Nd squares.

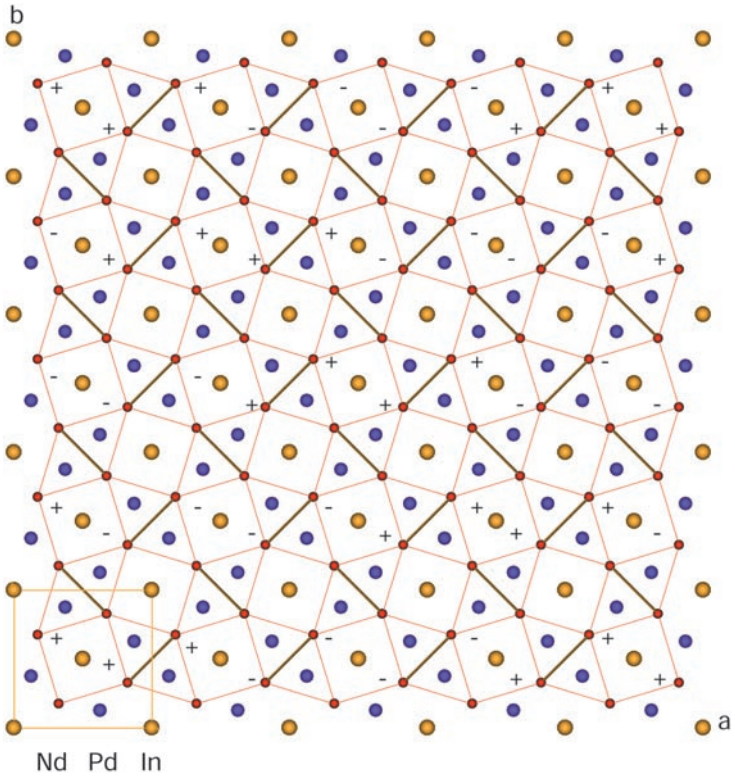

Figure 3. Chemical structure and magnetic unit cell of Nd_2Pd_2In projected onto the (a,b)-plane. The thicker bonds correspond to the shortest interatomic Nd–Nd distances. + and − indicate the orientation of the dominant magnetic Nd moments parallel and antiparallel to the c-axis, respectively.

Table 3. Structural parameters of Nd_2Pd_2In, refined according to space group $P4/mbm$ from neutron diffraction data taken at $T = 15$ K. Lattice parameters $a = 0.7719(1)$ nm, $c = 0.3861(1)$ nm. Occupation numbers 100% assumed, goodness of fit $\chi^2 = 2.16$, agreement value $R_{wp} = 4.76\%$, $R_{exp} = 3.24$, $R_I = 4.87\%$, 86 inequivalent reflections (hkl) contributing. Estimated standard deviations are given within parentheses.

Atom	Site	x	y	z	B [10^{-2} nm^2]
Nd	4h	0.1759(1)	0.6759(1)	0.5	0.0(1)
Pd	4g	0.3718(1)	0.8718(1)	0	0.16(3)
In	2a	0	0	0	0.57(7)

Table 4. Interatomic distances Nd–X [nm] in Nd_2Pd_2In, calculated from table 3.

Nd–2Pd	0.2885	Nd–Nd	0.3839
Nd–4Pd	0.3059	Nd–2Nd	0.3861
Nd–4In	0.3440	Nd–4Nd	0.4026

4. Magnetic ordering

4.1. Antiferromagnetism of Pr_2Pd_2In

At 1.6 K the neutron diffraction measurements performed on diffractometer D1B at ILL, Grenoble with a powder sample of Pr_2Pd_2In prove the existence of long-range

antiferromagnetic ordering of Pr. As illustrated in figure 4, the magnetic Bragg peaks correspond to the propagation vector $\boldsymbol{k} = [0, 0, 1/2]$, implying antitranslation along the c-axis.

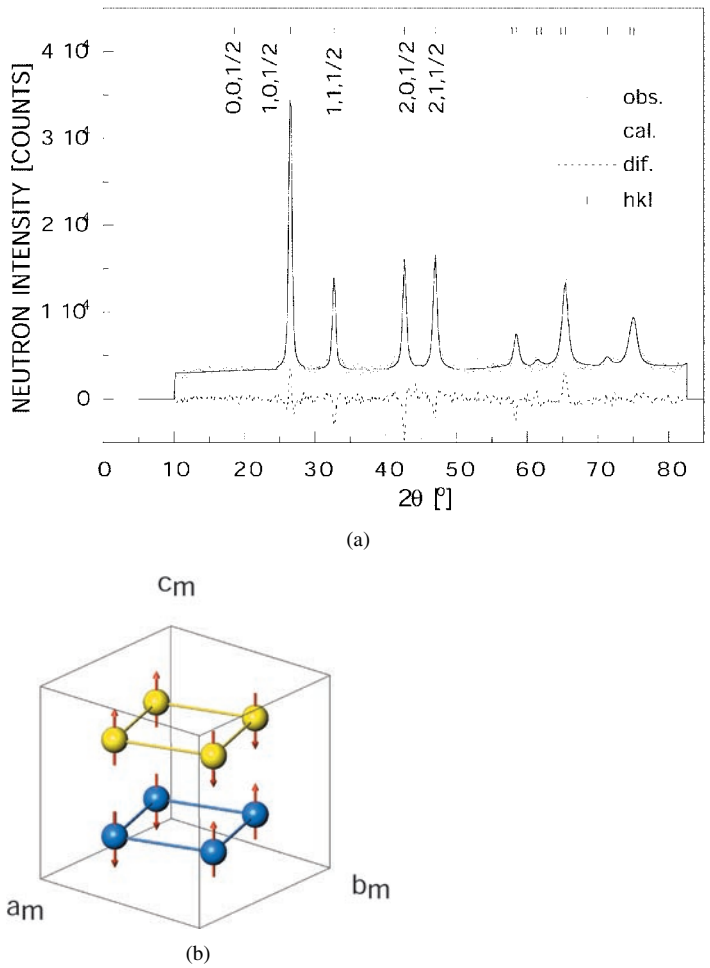

Figure 4. (a) Observed (I (1.6 K) − I (10 K) + 5000), calculated and difference magnetic neutron diffraction patterns of antiferromagnetic Pr_2Pd_2In (D1B data, $\lambda = 0.2518$ nm). Note that the largest magnetic peak is of the order of 10% of the largest nuclear Bragg peak. (b) Corresponding antiferromagnetic structure of Pr_2Pd_2In.

The results of a group theoretical symmetry analysis for this case, based on the program Mody [4], are summarized in table 5. Most of these magnetic configurations are already real and thus may be directly used. For the irreducible representation τ_9 one obtains with the order parameter $p = [(\mu/\sqrt{2})\,e^{i\varphi}, -i(\mu/\sqrt{2})\,e^{-i\varphi}]$ the real solutions $\boldsymbol{\mu}_1 = -\boldsymbol{\mu}_4 = \sqrt{2}\mu\boldsymbol{e}_z\cos(\varphi + \boldsymbol{k}\cdot\boldsymbol{t})$, $\boldsymbol{\mu}_2 = -\boldsymbol{\mu}_3 = -\sqrt{2}\mu\boldsymbol{e}_z\sin(\varphi + \boldsymbol{k}\cdot\boldsymbol{t})$, $\boldsymbol{e}_z$ = unit vector along the c-direction, $\boldsymbol{t}$ = translation vector of the chemical lattice. For constant magnitudes of the magnetic moments the phase φ should be $\pm\pi/4$. The two cases correspond to a $+-+-$ or $++--$ sequence of the magnetic moments of atoms 1 to 4. In the case of τ_{10} the order parameter $p = (c_1e^{i\varphi}, c_2e^{i\varphi}; ic_2e^{-i\varphi}, ic_2e^{-i\varphi})$ yields the real solutions $\boldsymbol{\mu}_1 = \boldsymbol{\mu}_4 = 2c_1\boldsymbol{e}_x\cos(\varphi+\boldsymbol{k}\cdot\boldsymbol{t})+2c_2\boldsymbol{e}_y\sin(\varphi+\boldsymbol{k}\cdot\boldsymbol{t})$, $\boldsymbol{\mu}_2 = \boldsymbol{\mu}_3 = -2c_2\boldsymbol{e}_x\cos(\varphi+\boldsymbol{k}\cdot\boldsymbol{t})+2c_1\boldsymbol{e}_y\sin(\varphi+\boldsymbol{k}\cdot\boldsymbol{t})$. The present results confirm those published previously by Bourée *et al* [5].

Table 5. Mody [4] results (apart from a common factor) of magnetic modes for Pr_2Pd_2In, space group No 127, $P4/mbm$, sites (4h): I: (0.18, 0.68, 0.5); II: (0.68, 0.82, 0.5); III: (0.32, 0.18, 0.5); IV: (0.82, 0.32, 0.5), $\boldsymbol{k} = [0, 0, 1/2]$, $\tau(12) = \tau_1(1) + \tau_2(1) + \tau_3(1) + \tau_5(1) + \tau_7(1) + \tau_8(1) + \tau_9(2) + 2\tau_{10}(2)$, $\boldsymbol{\mu}_j = e^{i\boldsymbol{k}\cdot\boldsymbol{t}} \sum_{l,n} c_{ln}\psi_{lmn}$, $e^{i\boldsymbol{k}\cdot\boldsymbol{t}} = e^{-i\boldsymbol{k}\cdot\boldsymbol{t}} = \cos(\boldsymbol{k}\cdot\boldsymbol{t})$; l refers to the irreducible representation, n to its dimension and m labels the basis vectors.

Site/mode	I	II	III	IV
Ψ_{111}	(1, −1, 0)	(−1, −1, 0)	(1, 1, 0)	(−1, 1, 0)
Ψ_{231}	(0, 0, 1)	(0, 0, 1)	(0, 0, 1)	(0, 0, 1)
Ψ_{311}	(1, 1, 0)	(1, −1, 0)	(−1, 1, 0)	(−1, −1, 0)
Ψ_{511}	(1, 1, 0)	(−1, 1, 0)	(1, −1, 0)	(−1, −1, 0)
Ψ_{711}	(1, −1, 0)	(1, 1, 0)	(−1, −1, 0)	(−1, 1, 0)
Ψ_{831}	(0, 0, 1)	(0, 0, −1)	(0, 0, −1)	(0, 0, 1)
Ψ_{931}	(0, 0, 1)	(0, 0, i)	(0, 0, −i)	(0, 0, −1)
Ψ_{932}	(0, 0, i)	(0, 0, 1)	(0, 0, −1)	(0, 0, −i)
Ψ_{1011}	(1, 0, 0)	(0, −i, 0)	(0, −i, 0)	(1, 0, 0)
Ψ_{1012}	(0, −i, 0)	(−1, 0, 0)	(−1, 0, 0)	(0, −i, 0)
Ψ_{1021}	(0, 1, 0)	(i, 0, 0)	(i, 0, 0)	(0, 1, 0)
Ψ_{1022}	(−i, 0, 0)	(0, 1, 0)	(0, 1, 0)	(−i, 0, 0)

Table 6. Comparison of observed and calculated (τ_9) integrated magnetic intensities for Pr_2Pd_2In at $T = 1.6$ K.

hkl	2θ [°]	I_{obs}	ΔI_{obs}	I_{cal}
0, 0, 1/2	18.56	0	500	0
1, 0, 1/2	26.51	22 330	1243	22 104
1, 1, 1/2	32.68	7342	1237	7663
2, 0, 1/2	42.66	10 351	1281	10 630
2, 1, 1/2	46.98	12 739	1338	11 788
0, 0, 3/2	57.85	0	500	0
2, 2, 1/2	58.48	3092	1832	4494
1, 0, 3/2	61.38	640	624	813
3, 0, 1/2	61.99	82	323	276
1, 1, 3/2	64.80	504	95	532
3, 1, 1/2	65.39	12 663	1488	12 575
2, 0, 3/2	71.37	1143	1003	1500
2, 1, 3/2	74.55	2100	380	2082
3, 2, 1/2	75.11	8466	1327	8038

Best agreement (concerning integrated nuclear and magnetic neutron intensities: $R_{IN} = 5.1\%$, $R_{IM} = 9.7\%$, excluding the scattering angle range 2θ from 71.2 to 73.4°, which caused minor problems in the nuclear fit at 10 K, perhaps due to contamination by a Cu(111) peak) of observed and calculated nuclear and magnetic D1B neutron intensities, at 1.6 K, was obtained for the configuration ++−− corresponding to the irreducible representation τ_9. The +−+− sequence yielded $R_{IM} = 13.0\%$. In particular for magnetic difference patterns we obtained better fits with an X parameter instead of a Y parameter used for the nuclear peak shape with function 7 (Lorentzian contribution to the peak half width proportional to $X \tan\theta + Y/\cos\theta$) [3]. The corresponding magnetic difference pattern ($R_{IM} = 5.5\%$ including all magnetic peaks) and the resulting magnetic structure are shown in figure 4. In table 6 corresponding observed and calculated integrated magnetic neutron intensities are compared. The magnitude of the ordered magnetic Pr moment at 1.6 K amounts to $\mu_{Pr} = 1.8(3)\ \mu_B$. We cannot exclude completely the possibility of a certain tilt of the magnetic moments from the c-axis by a ζ angle

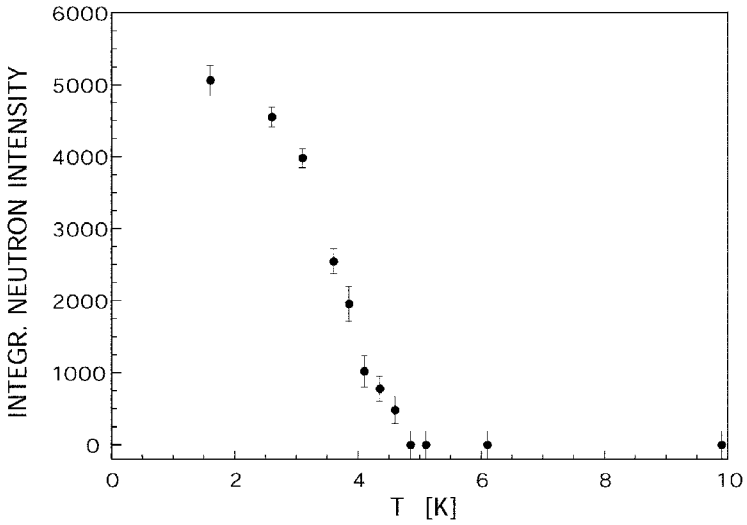

Figure 5. Temperature dependence of the integrated magnetic neutron intensity of the magnetic Bragg peak (3, 1, 1/2) of Pr_2Pd_2In.

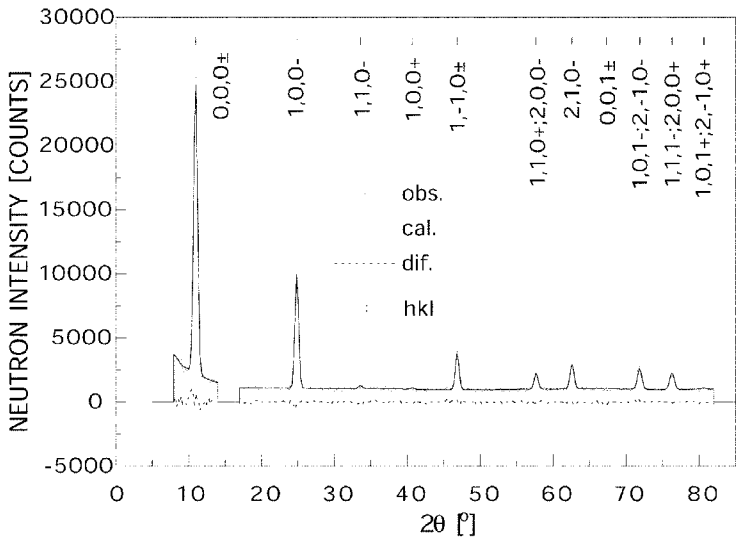

Figure 6. Observed (I(2.2 K) − I(15 K) + 1000, DMC data, $\lambda = 0.422$ nm), calculated and difference magnetic neutron diffraction patterns of Nd_2Pd_2In. The excluded angular region between the first two magnetic Bragg peaks of Nd_2Pd_2In is due to a very weak magnetic peak which most probably originates from the minor second phase.

up to 30°, but we do not think that this is significant ($R_{IN} = 5.3\%$, $R_{IM} = 8.7\%$; $R_{IM} = 13.0\%$ for the difference fit similar to figure 4). The absence of magnetic peaks such as (0, 0, 1/2) also suggests the orientation of the magnetic Pr moment along the c-axis, i.e. parallel to $\boldsymbol{k}$.

The temperature dependence of the integrated magnetic neutron intensity of the magnetic Bragg peak (3, 1, 1/2) is shown in figure 5. It indicates a Néel temperature of 5.0(5) K, in good agreement with bulk magnetic measurements [1].

Table 7. Possible magnetic modes for space group $P4/mbm$ (No 127) in the case of R sites (4h) of Nd_2Pd_2In for propagation vectors $\boldsymbol{k}_1 = [x, x, 0]$, $x = 1/4$ and $\boldsymbol{k}_4$, which is equivalent to $-\boldsymbol{k}_1$, as obtained by the program Mody [4]. τ = irreducible representation; $\boldsymbol{k}_1 = [1/4, 1/4, 0]$, $\boldsymbol{k}_2 = [1/4, 3/4, 0]$, $\boldsymbol{k}_3 = [3/4, 1/4, 0]$, $\boldsymbol{k}_4 = [3/4, 3/4, 0]$; $\tau(12) = \tau_2(1) + \tau_3(1) + \tau_4(1)$; $\tau_1(1) + 2\tau_2(1) + \tau_3(1) + 2\tau_4(1)$; $\tau_2(1) + \tau_3(1) + \tau_4(1)$.

Mode		(0.18, 0.68, 1/2)	(0.68, 0.82, 1/2)	(0.32, 0.18, 1/2)	(0.82, 0.32, 1/2)
τ_1: $\boldsymbol{k}_1$, orbit 2	$^1\Psi_{123}$		(0, 0, 1)	(0, 0, i)	
$\boldsymbol{k}_4$, orbit 2	$^4\Psi_{123}$		(0, 0, −i)	(0, 0, −1)	
τ_2: $\boldsymbol{k}_1$, orbit 1	$^1\Psi_{211}$	(1, 1, 0)			
$\boldsymbol{k}_1$, orbit 2	$^1\Psi_{221}$		(1, 0, 0)	(0, −i, 0)	
$\boldsymbol{k}_1$, orbit 2	$^1\Psi_{222}$		(0, 1, 0)	(−i, 0, 0)	
$\boldsymbol{k}_1$, orbit 3	$^1\Psi_{231}$				(1, 1, 0)
$\boldsymbol{k}_4$, orbit 1	$^4\Psi_{211}$				(1, 1, 0)
$\boldsymbol{k}_4$, orbit 2	$^4\Psi_{221}$		(0, −i, 0)	(1, 0, 0)	
$\boldsymbol{k}_4$, orbit 2	$^4\Psi_{222}$		(−i, 0, 0)	(0, 1, 0)	
$\boldsymbol{k}_4$, orbit 3	$^4\Psi_{231}$	(1, 1, 0)			
τ_3: $\boldsymbol{k}_1$, orbit 1	$^1\Psi_{313}$	(0, 0, 1)			
$\boldsymbol{k}_1$, orbit 2	$^1\Psi_{323}$		(0, 0, 1)	(0, 0, −i)	
$\boldsymbol{k}_1$, orbit 3	$^1\Psi_{333}$				(0, 0, 1)
$\boldsymbol{k}_4$, orbit 1	$^4\Psi_{313}$				(0, 0, −1)
$\boldsymbol{k}_4$, orbit 2	$^4\Psi_{323}$		(0, 0, i)	(0, 0, −1)	
$\boldsymbol{k}_4$, orbit 3	$^4\Psi_{333}$	(0, 0, −1)			
τ_4: $\boldsymbol{k}_1$, orbit 1	$^1\Psi_{411}$	(1, −1, 0)			
$\boldsymbol{k}_1$, orbit 2	$^1\Psi_{421}$		(1, 0, 0)	(0, i, 0)	
$\boldsymbol{k}_1$, orbit 2	$^1\Psi_{422}$		(0, 1, 0)	(i, 0, 0)	
$\boldsymbol{k}_1$, orbit 3	$^1\Psi_{431}$				(1, −1, 0)
$\boldsymbol{k}_4$, orbit 1	$^4\Psi_{411}$				(1, −1, 0)
$\boldsymbol{k}_4$, orbit 2	$^4\Psi_{421}$		(0, i, 0)	(1, 0, 0)	
$\boldsymbol{k}_4$, orbit 2	$^4\Psi_{422}$		(i, 0, 0)	(0, 1, 0)	
$\boldsymbol{k}_4$, orbit 3	$^4\Psi_{431}$	(1, −1, 0)			

4.2. Antiferromagnetic ordering of Nd_2Pd_2In

Figure 6 shows a magnetic difference pattern for Nd_2Pd_2In, measured on DMC with neutron wavelength $\lambda = 0.422$ nm to detect satellite peaks at small scattering angles. Pattern matching [3] for $\boldsymbol{k} = [1/4, 1/4, 0]$ yields an excellent fit, suggesting this $\boldsymbol{k}$-vector for Nd_2Pd_2In. Earlier D1A measurements on this compound with $\lambda = 0.1911$ nm also indicated the same $\boldsymbol{k}$-vector.

Group theoretical symmetry analysis for this case is summarized in table 7. The magnetic modes correspond to three independent orbits. To obtain real solutions, one has to find linear combinations of the basis vectors by combining the wavevectors $\boldsymbol{k}_1$ and $\boldsymbol{k}_4$ [2], which yield satisfactory agreement of calculated and observed magnetic neutron intensities.

The dominant $000_\pm$ satellite suggests orientation of the magnetic moments perpendicular to $\boldsymbol{k}$, i.e. parallel to the c-axis. Using the order parameters [2] $p_1 = [a\,e^{i\alpha}, -a\,e^{-i\alpha}]$, $p_2 = [-bi\,e^{i\beta}, b\,e^{-i\beta}]$, $p_3 = [c\,e^{i\gamma}, -c\,e^{-i\gamma}]$ for the three orbits in case of the irreducible representation τ_3, one obtains:

$$\boldsymbol{\mu}_1 = \boldsymbol{e}_z 2a\cos(\alpha + \boldsymbol{k}\cdot\boldsymbol{t}) \qquad \boldsymbol{\mu}_2 = \boldsymbol{e}_z 2b\cos(\beta - \pi/2 + \boldsymbol{k}\cdot\boldsymbol{t})$$
$$\boldsymbol{\mu}_3 = -\boldsymbol{e}_z 2b\cos(\beta + \boldsymbol{k}\cdot\boldsymbol{t}) \qquad \boldsymbol{\mu}_4 = \boldsymbol{e}_z 2c\cos(\gamma + \boldsymbol{k}\cdot\boldsymbol{t}).$$

For equal magnetic moments at all equivalent Nd positions, the phases should be $\pm\pi/4$.

Refinement of these parameters and of the amplitudes converged to $c = a$, $\alpha = -\pi/4 = -\beta = -\gamma$. This yields in the chemical unit cell within error limits the free ion value gJ [μ_B]

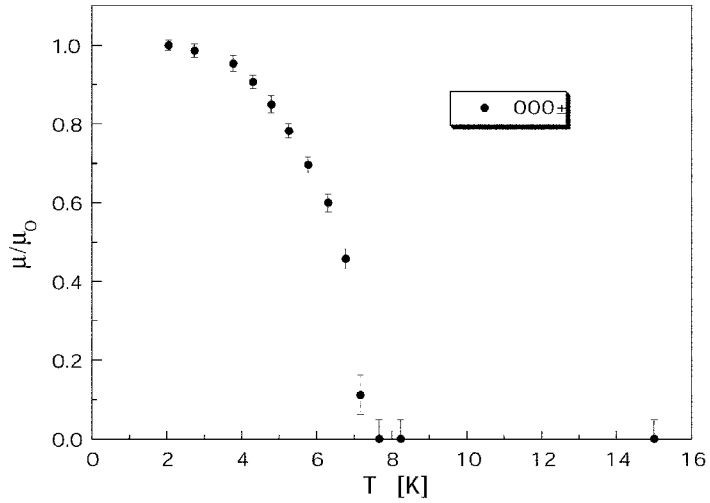

Figure 7. Temperature dependence of the average reduced ordered magnetic Nd moment of Nd_2Pd_2In, determined from DMC measurements.

of 3.3(2) μ_B for $\mu_1 = \mu_4$ and $\mu_2 = -\mu_3 = 0.8(1)\ \mu_B$. The excellent fit with goodness of fit $\chi^2 = 1.6$ and $R_{IM} = 3.9\%$ is shown in figure 6, and the corresponding modulated magnetic structure is illustrated in figure 3. With the constraint of constant Nd moment magnitude on all four sites only $R_{IM} = 24\%$ resulted with $\mu \approx 3.3\ \mu_B$.

The temperature dependence of the average reduced ordered magnetic Nd moment (square root of the integrated $000_{\pm}$ neutron intensity) is shown in figure 7, indicating a Néel temperature $T_N = 7.5(5)$ K, in fair agreement with the value of 8 K known from bulk magnetic measurements [1].

5. Discussion and conclusions

The intermetallic rare-earth compounds Pr_2Pd_2In and Nd_2Pd_2In with tetragonal Mo_2FeB_2 type chemical structures show at low temperatures commensurate antiferromagnetic rare earth ordering of modulated type corresponding to $\boldsymbol{k} = [0, 0, 1/2]$ and $[1/4, 1/4, 0]$, respectively. To our knowledge the latter type of magnetic ordering has not yet been observed in such systems. The magnetic moments appear to be oriented parallel to the c-axis. As incommensurate modulated magnetic ordering with $\boldsymbol{k} \approx [0.22, 0, 0]$ had been determined for antiferromagnetic and $\boldsymbol{k} = [0, 0, 0]$ for ferromagnetic, nonstoichiometric Ce_2Pd_2In compounds, the R_2Pd_2In series displays a remarkable variation of magnetic ordering. The latter compounds show features of highly correlated electron systems [1]. Similarly $U_2(Ni_{1-x}Pt_x)_2In$, which for $x \leqslant 0.5$ crystallizes also with $P4/mbm$ symmetry, has recently been reported to be a dense Kondo system [6]. For $x = 0$ and 0.2 $\boldsymbol{k} = [0, 0, 1/2]$ was found with magnetic U moments oriented perpendicular to the c-axis, while for $x = 0.5$ incommensurate U ordering with $\boldsymbol{k} = [0, 0, 0.56]$ was observed. With respect to R_2Pd_2Sn rare-earth compounds it is remarkable that $Tb_2Pd_{2.05}Sn_{0.95}$ has been reported by Laffargue *et al* [7] to order magnetically with $\boldsymbol{k}_2 = [0, 0, 1/2]$ in a τ_{10} configuration below $T_2 = 20.8$ K, whereas $\boldsymbol{k}_1 = [k_x, k_x, 1/2]$ with k_x varying from 0.115 at 26.3 K ($T_N = 27.3$ K) to 0.070 at $T = 20.8$ K was observed. Apart from crystal field effects usually determining the easy directions of magnetization in rare-earth compounds, the change in magnetic ordering is presumably due to variations of

the rare-earth R–R distances because of the lanthanide contraction, which modify the RKKY exchange interactions depending on the distances. For example the shortest Pr–Pr distance parallel to the (a,b)-plane is comparable to the second shortest Nd–Nd distance parallel to the c-axis (see tables 2 and 4). Presumably this is the reason for antitranslation along this direction in case of Pr_2Pd_2In and ferromagnetic coupling perpendicular to the (a, b)-plane for Nd_2Pd_2In. As illustrated in figure 3, the Mo_2FeB_2 type chemical structure tends to frustration effects in magnetic ordering. This may cause the substantial differences found in the ordered magnetic moment values of the Nd^{3+} ions (1, 4) and (2, 3) within the chemical unit cell. Figure 3 indicates dominant magnetic Nd–Nd coupling along $\langle 1, 0, 0\rangle$-chains via the shortest Nd–Nd distances. The ordered magnetic Nd(1) and Nd(4) moments of Nd_2Pd_2In at saturation correspond within error limits to the free ion value 3.27 μ_B of Nd^{3+} with a $^4I_{9/2}$ ground multiplet. The small magnetic moments of Nd(2) and Nd(3) are presumably due to frustration effects. On the other hand the ordered magnetic Pr moment of Pr_2Pd_2In at saturation of 1.8(3) μ_B is considerably smaller than the free ion value 3.20 μ_B of Pr^{3+} with $^3H_4$ ground multiplet, which indicates a large crystal-field reduction. The temperature dependencies of the ordered magnetic moments display second-order phase transitions at the Néel temperatures T_N of 5 and 8 K for R = Pr and Nd, respectively, in agreement with bulk magnetic measurements [1]. In summary one may conclude that the isostructural series of R_2Pd_2In compounds of trivalent rare earths R exhibits a remarkable variation in magnetic rare-earth ordering.

Acknowledgments

For financial support of the present work we are indebted to the Swiss National Science Foundation. We thank Professor A Furrer, LNS for his interest in the present work and Professor W Sikora, The University of Mining and Metallurgy, Krakow for a new version of the program Mody and for important advice concerning its use.

References

[1] Giovannini M, Michor H, Bauer E, Hilscher G, Rogl P and Ferro R 1998 *J. Alloys Compounds* **280** 26
[2] Giovannini M *et al* 2000 *Phys. Rev.* B **61** 4044
[3] Rodriguez-Carvajal J 1993 *Physica* B **192** 55
[4] Sikora W 1999 *Symmetry and Structural Properties of Condensed Matter, Zajaczkowo* ed T Lulek *et al* (Singapore: World Scientific) p 484
[5] Bourée F, Chevalier B, Fournès L, Mirambet F, Roisnel T, Tran V H and Zolnierek Z 1994 *J. Magn. Magn. Mater.* **138** 309
[6] Tran V H, Hoser A and Hofmann M 2000 *J. Phys.: Condens. Matter* **12** 1029
[7] Laffargue D, Roisnel T, Chevalier B and Bourée F 1997 *J. Alloys Compounds* **262/263** 219